

A High Temperature Electrostatic Levitator for 1-g

Won-Kyu Rhim, Sang K. Chung, Daniel Barber, Kin F. Man, Gary Gutt,
Aaron Rulison[†], and R. Erik Spjut^{††}

Jet Propulsion Laboratory, California Institute of Technology
4800 Oak Grove Drive, Pasadena, CA 91109

Abstract

Recent developments in high temperature electrostatic levitation technology for containerless processing of metals and alloys is described. This is the first demonstration in which metals and alloys can be levitated and melted in vacuum. The superheating-undercooling-recrystallization cycles can be repeated while maintaining good positioning stability. Besides providing good positioning stability and an open sample view, the present levitator is capable of varying sample temperatures without affecting the levitation. This paper also describes the general architecture of the experimental hardware and software, sample heating and charging, and the operational procedure. The system performance is demonstrated by showing multiple superheating-undercooling-recrystallization cycles in a zirconium sample ($T_m = 2128$ K). While the present levitator is oriented toward ground-based operation, it is possible to extend it for applications in microgravity.

† NASA- NRC Resident Research Associate

†† Department of Engineering, Harvey Mudd College, Claremont, CA

Introduction

The studies of thermophysical properties of undercooled liquid states, nucleation kinetics, and the production of various metastable phases in different materials often require the processing of materials in a containerless environment. The electrostatic levitator described in this paper provides the capability of superheating, undercooling, and solidifying metals and alloys in a clean (contactless and high vacuum) and quiescent

environment. This levitator is an extension of the one previously described¹ in which sample levitation was limited to low density materials at ambient conditions.

The present high-temperature, high-vacuum, electrostatic levitator (ESL) has several important advantages over the electromagnetic levitator (EML)², the only alternative technique having similar capabilities: (i) The ESL can, in principle, levitate a broad range of materials, including metals, semiconductors and insulators. Since maintaining a sufficient surface charge on the sample is the only requirement to generate a levitation force. In contrast, materials that the EML can levitate are limited primarily to electrical conductors. (ii) In an ESL, sample heating and levitation do not interfere with each other so that the sample temperature can be varied over a wide range; whereas the electromagnetic field in an EML is intrinsically coupled to sample heating, which limits the lowest temperature it can attain for a given sample density. (iii) The ESL, through employment of feedback control, provides quiescent positioning during sample processing; whereas a molten sample levitated by an EML is subjected to strong internal flow which may cause severe shape distortion, prevents accurate temperature measurements, and perhaps causes premature nucleation, therefore preventing deeper undercooling. (iv) The ESL provides a more open view; whereas the levitation and heating coils in an EML are closely wound around the levitated sample, severely restricting access to the diagnostic instruments. However, the ESL does require either a high vacuum or a high pressure environment in order for a high electric field to be applied without causing gas breakdown.

This paper describes the principles of electrostatic levitation, the experimental hardware and software, sample charging, and the operational procedure. The system is demonstrated by showing results of zirconium undercooling experiments.

The Principles of Electrostatic Levitation

Since a three-dimensional electrostatic potential minimum does not exist (Earnshaw's theorem³), electrostatic sample positioning is only possible with an actively controlled applied electric field. In our system

this was accomplished using a feedback-control whereby any deviation in sample position from a preset position was automatically corrected. Fig. 1 shows a schematic diagram of an electrostatic levitator with one-dimensional control capability. It employs a single-axis position control along the vertical direction to overcome the gravitational acceleration, g . The error between the vertical position and the preset z -coordinate is processed by a computer (according to a feedback algorithm) to generate a control signal and apply it to the top electrode to maintain the sample at the preset position. The force-balance equation for levitation when the sample is positioned at the center of a pair of infinite parallel electrodes is given approximately by:

$$mg = Q_s V / l, \quad (1)$$

where m is the mass of the sample carrying a charge Q_s , and V is the voltage difference between the two electrodes separated by a distance l . For $Q_s = 0.69 \times 10^{-9}$ C, $m = 140$ mg, and $l = 10$ mm, V is approximately -10 kV.

As explained in reference 4, the electrode arrangement shown in Fig. 1 provides a two-dimensional potential well in the horizontal direction when it is operated in the presence of a gravitational force on Earth, but in the microgravity environment of space such a potential well does not exist and the ESL would require a different electrode arrangement and control method.

The Experimental Hardware

A schematic diagram of the present high temperature/high vacuum electrostatic levitator is shown in Fig. 2, and a photograph of the vacuum chamber with a sample being levitated between a pair of electrodes is shown in Fig. 3. The electrode assembly is positioned at the center of the chamber and all the necessary equipment for levitation, heating, and diagnostics are located around the chamber. The chamber is evacuated to an ultimate vacuum of 5×10^{-8} Torr by a vibration-free magnetically

suspended turbo-molecular pump (Osaka model "1'1 1250M) backed by a roughing pump (Danielson model TD 1 00).

The electrode assembly used in the present levitator has two pairs of side electrodes surrounding the bottom electrode (Fig. 4). Damping voltages applied on these side electrodes prevent sample oscillation in the lateral direction. The hole at the center of the bottom electrode allows access to the sample storage-manipulation system located below the electrode. The system can stem up to 12 samples in a carousel inside the high vacuum chamber. It contains a sample recovery system so that if a sample should drop out of the ESL, it will land in a ceramic cone, roll to the center, and from there can be lifted back to the ESL or lowered into the carousel. All of these actions can be accomplished while maintaining a high vacuum in the chamber.

Two orthogonal HeNe lasers (30 mW each) together with two position detectors provide the 3-dimensional position information which is used by the microcomputer to generate a feedback signal. A Macintosh IIx computer and 12 bit A/D, D/A cards were used for data acquisition and position control. The computer is equipped with a Motorola 50 MHz 68030 microprocessor and 68882 floating point math coprocessor. The 12 bit A/D and D/A cards from National Instruments fit into the Nubus inside the computer. The three position signals (produced by the two orthogonally-positioned detectors) are fed into the computer through an A/D card, and after going through the control routine the three output signals are sent to the high voltage amplifiers through a D/A card. The position sensitive detectors (HAMAMATSU model C2399-01) are commercially available. This type of detector is normally used for sensing a bright image on a dark background. In this system, however, due to the xenon lamp light (used for heating) which brightly illuminates the chamber and the sample, they are being used in a reversed mode (dark image on a bright background). This was accomplished by adding a collimated HeNe laser beam in the background and attaching a matching narrow band filter in front of the detector to pass only the light of the laser wavelength while stopping the light coming from the xenon lamp. The computer converts the detector output to the actual sample position.

Sample heating is provided by a 1 - kilowatt UV - rich high-pressure xenon arc lamp (ILC, model LX 1000CF). The radiation produced by the

bulb is roughly collimated into a 5 cm beam by a parabolic reflector at the back of the bulb housing. The beam is then focused by a 7.5 cm focal length fused quartz lens into a small spot in order to maximize the light flux on the sample. Since the beam originates from a finite discharge gap between the anode and the cathode and not from a point source, the focused spot size could not be reduced to less than 5 mm. Fused quartz was used in order to transmit the UV component of the xenon beam for sample charging via the photoelectric effect. (Sample charging by UV will be described below.) A fused quartz mirror, 7.5 cm both in diameter and in radius of curvature, is placed opposite the lens. This mirror collects most of the xenon light beam that misses the sample. The temperature of a 2.5 mm diameter zirconium sphere could be varied from room temperature to 2270 K by adjusting the iris in front of the xenon lamp. Without the mirror, the maximum temperature could not exceed 1750 K.

The sample temperature was measured using a home-built single-color pyrometer which was constructed and calibrated according to the prescription provided by Hofmeister et al.⁶. The pyrometer collects the radiative power emitted by a well-defined area on the sample surface into a certain solid angle and over a small wavelength range (10 nm band width at 658 nm wavelength). Given certain assumptions about the sample's directional spectral emissivity, the collected power can be converted to sample temperature through Planck's equation for the spectral distribution of emissive power if the pyrometer output corresponding to one temperature is known, typically at the sample melting point. For zirconium, the rapid increase in temperature to the melting point as a result of recalescence provides an easily recognized reference point, allowing the temperature to be calculated *a posteriori* for the entire undercooling experiment. Data acquisition was by a Macintosh II computer with a National Instruments A/D converter. The driving software automatically recognizes the reference temperature, T_{ref} , by searching for the rapid increase in the pyrometer output associated with recalescence. It then calculates the temperature for the entire experiment and provides a plot of temperature versus time. The percentage of undercooling and other important parameters are also computed and displayed.

A close-up view of the sample was videotaped during the experiments using a camera with a telephoto lens.

The Position Control Software

The architecture of the position control software is shown in Fig. 5 in a flow-chart format. The software is divided into two groups: FOREGROUND and BACKGROUND. The foreground tasks consist of the servo control and the data collection that require synchronized operations with highest priority. The background tasks consist of a user interface, inputs from a keyboard and mouse, and graphics, which are given secondary priority. Data files can also be created and saved onto the hard drive through the background mode. These two modes of operation are made possible by the use of the interrupt request capability of the Macintosh computer. When an interrupt signal is issued (from an external programmable pulse generator) the computer sets aside background routines, stores the present state of its registers into memory, and launches the foreground routine. During the foreground routine, the position information is collected from an A/D, the control algorithm is computed, a proper servo control value is sent out through a D/A, and a single frame of data is collected into a specified memory buffer. After the foreground routine is successfully executed, the computer recaptures its previous register values and continues with its background task. This process is set into a continuous loop with an interrupt frequency of 480 Hz.

The vertical axis servo control utilizes the commonly used PID (Proportional, Integral, Derivative) algorithm⁶. Since the horizontal plane has a passive potential minimum it does not normally require an active feedback control. In vacuum, however, there is no gas medium to damp out horizontal oscillations, so a horizontal controller, consisting of two sets of side electrodes, was used to provide lateral damping. The vertical control is executed in every loop whereas the horizontal control is executed ten times slower. The actual stability of the sample has been found to depend strongly on vibrations from the floor. A stability better than 20 μm was achieved for a 3 mm sample with a specific density of 8, carrying a constant charge.

The user interface consists of keyboard and mouse inputs and a graphics display. The keyboard and mouse are used for entering servo and

other necessary parameters for proper data acquisition. It can, therefore, interrupt the loop at any time, although the servo-loop has a high priority. The graphics display consists of sample positions, control voltage outputs and temperature readings (Fig. 6). The programs were written in the 'C' language except the interrupt handler routine which was written in assembly Code.

Sample Charging

Sample charging is a critical part, of electrostatic positioning. The amount of charge on the sample surface determines the positioning force that can be imparted on the sample with a given electrostatic field. Three charging methods that are relevant during different phases of processing have been employed: capacitive, photoelectric and thermionic charging.

a. Numerical Analysis of Capacitive Charging

A general-purpose three-dimensional computer model was created to determine the potential, charge, and force distributions on a sample in an electrostatic levitator. Since an analytical solution of this system with arbitrary sample and electrode geometries is impractical, this model uses a numerical finite-difference approach. The potential and charge distributions are obtained using a Multigrid Method solver⁷ and the forces on the sample are derived from these distributions. This model allows us to evaluate and optimize different electrode configurations for the levitator.

The relationships between the parameters (e.g. sample size, position, density, charge, forces, and electrode potentials) that are obtained from this model are shown in Figs. 7 and 8 to give some insights into this system. In all of the examples the levitator consists of circular top and bottom disk electrodes, separated by 8 mm, with the top electrode connected to a 1 kV amplifier while the bottom electrode is grounded. The sample was assumed to be spherical (see Fig. 9(a)).

Fig. 7(a) shows the top electrode potential as a function of sample density and diameter at the moment of launch. The corresponding induced charge on the sample is shown in Fig. 7(b). The top electrode potential needed to levitate the sample midway between the electrodes is presented in Fig. 8, where the sample is assumed to have retained the charge

acquired at launch. For example, a sample with a density 10 and diameter 3 mm which is initially placed at the center of the bottom electrode (Fig. 9(a)) will jump off the bottom electrode when the top electrode voltage reaches ~ -14.5 kV (from Fig. 7(a)) and carry an induced charge of -0.8 nC (from Fig. 8), and when the sample is levitated midway between the electrodes the voltage will be ~ -13 kV (from Fig. 7(b)).

b. Qualitative Analysis of Photoelectric, Thermionic, and Surface Ionization Charging

When a cold sample is launched with initial charge Q_s , it requires a levitation voltage given approximately by Eqn. (1). However, V is subjected to change as Q_s changes. In fact this is what happens when the sample is subjected to the various charging mechanisms mentioned above. When the sample is heated by a focused xenon lamp beam, the UV component ejects electrons not only from the sample but also from surrounding materials as a result of reflection and scattering. Surface ionization of outgassing materials⁸ causes loss of sample charge. Thermionic emission of electrons occurs at elevated temperatures. The equilibrium charge of a levitated sample is established through the balance of electrical currents flowing between the sample and electrodes.

Consider the case in which the sample has reached a steady-state temperature and is positional between the top electrode (at a negative potential V) and the bottom electrode (grounded). A current I_p (taken to be positive for electrons leaving the sample) flowing from the sample to the bottom electrode may be expressed by

$$I_p = -V_s/R_p \quad (2)$$

where V_s is the sample potential and R_p is defined as the equivalent resistance for flow of charge from the sample to the bottom electrode; R_p decreases with increasing xenon lamp intensity. It also decreases with increasing sample temperature due to thermionic emission of electrons.

Similarly, the current flowing from the top electrode to the sample (taken to be positive for electrons leaving the top electrode) is

$$I_u = (V_s - V)/R_u \quad (3)$$

where R_u is defined as the equivalent resistance for flow of current from the top electrode to the sample; R_u decreases with increasing xenon lamp intensity and increasing positive surface ionization of outgassing materials.

The present situation may be represented by an equivalent resistance-capacitance circuit (Fig. 9(b)) where C_u and C_p are the mutual capacitances between the sample and the top and the bottom electrodes, respectively. Therefore, the sample charge is given by

$$\begin{aligned} Q_s &= Q_p - Q_u \\ &= C_p V_s - C_u (V - V_s) \\ &= (C_p + C_u) V_s - C_u V. \end{aligned} \quad (4)$$

where Q_p is the charge on C_p , and Q_u is the charge on C_u . If the sample is spherical and has established a steady state charge while it is levitated midway between the electrodes (so that $C_p \approx C_u \equiv C$), then the solutions of the equivalent circuit for the sample charge, Q_{ss} , and the required levitation voltage, V_f , are given by:

$$Q_{ss}^2 = mglC \frac{1 - \alpha}{1 + \alpha}, \quad (5)$$

and,

$$V_f^2 = \frac{mgl}{C} \frac{1 + \alpha}{1 - \alpha}, \quad (6)$$

with

$$\alpha \equiv R_p/R_u. \quad (7)$$

These two equations are plotted in Fig. 10. Notice that the sample charge holds its largest value, \sqrt{mglC} , when $\alpha = 0$, requiring the lowest electrode voltage, and the sample holds no charge if $\alpha = 1$, requiring an infinite electrode voltage. This means that in order to maintain a sufficient charge for levitation, one must control R_u and R_p so that α is 'sufficiently small'.

At high temperature the thermionic emission dominates, thus easily satisfying this requirement. Therefore, the major concern for sample levitation may arise in the lower temperature range where thermionic

emission is insignificant and the sample charging depends solely on the relative magnitude between the (charging) photoelectric current and the (discharging) surface ionization currents. The effect of outgassing can be reduced by allowing more gradual outgassing as the sample temperature is raised more slowly.

Operational Procedure

Up to 12 clean samples were loaded into the sample storage carousel and the chamber evacuated to 10^{-7} Torr. The position control software was turned on and the appropriate set position and PG, I₁~~, and IG gains were keyed in. A Trek 20 kV amplifier (model 620A) was used for the z-axis control and two Trek 10 kV amplifiers (model 609A) were used for the x- and y-axis clamping. As soon as the top electrode reached a threshold voltage the sample jumped away from the bottom electrode toward the set position. Minor adjustments to the gains and set point were then made to establish the most quiescent levitation conditions. The stability was typically better than 20 μ m at this point.

The iris in front of the xenon lamp was then opened gradually while the levitation voltage was being monitored. Changes in the sample charge were manifested by corresponding changes in levitation voltage according to Eqn. (1). If a substantial charge decrease occurred, the iris was adjusted so that the required levitation voltage remained within the range of the high voltage amplifiers (± 20 kV in this case). As the sample charge changed during heating, the control gains were frequently adjusted in order to maintain the best position stability.

System Performance in an Undercooling Experiment

Once the sample melted and reached the desired superheated temperature, it was ready for an undercooling experiment. In a vacuum environment the change in internal energy of the sample is equal to the difference between the heat arriving from the xenon beam and that lost due to radiation:

$$\rho V C_p dT/dt = Q_{in} - A\sigma\epsilon_T(T^4 - T_b^4), \quad (8)$$

where p is the sample density, V is the volume, C_p is the heat capacity, Q_{in} is the heat due to the beam, A is the sample surface area, σ is the Stefan-Boltzmann constant, ϵ_T is the total hemispherical emissivity, " T " is the sample temperature, and " T_b " is the background temperature. This formulation assumes that the background acts as a blackbody, which is true in most cases where the sample chamber is much larger than the sample. The steady state temperature, T_f , is then given by:

$$T_f = (Q_{in}/A\sigma\epsilon + T_b^4)^{1/4} \quad (9)$$

If the xenon beam is turned off, then $Q_{in} = 0$ in Eqn. (8), and T_f will decay to " T_b " due to radiative cooling. Fig. 11 shows a photograph of molten drop of zirconium (density = 6.49 g/cm³) being levitated at " $T_f = 2250$ K (120 K above its melting temperature) in the presence of a heating beam. The sample diameter was approximately 2.3 mm. The highlight spots seen on the sample disappeared when the beam was turned off. Fig. 12 shows a temperature versus time curve of the same sample when the heating beam was suddenly removed at the sample temperature of 2250 K. Before the beam was removed the Pyrometer was strongly influenced by reflected radiation, showing a high level of noise as seen at the beginning of the curve. Therefore, the temperature reading is inaccurate while the lamp is on. As soon as the beam is blocked the sample underwent radiative cooling according to Eqn. (8) (with $Q_{in} = 0$) until recalescence occurred. Recalescence is marked by a sudden increase in temperature to its melting point as the sample releases its latent heat. The liquid-solid coexistence period lasted for approximately 0.3 seconds before the sample temperature decayed again. The data presented in this figure was obtained by digitizing the pyrometer output at 1 kHz.

Since $(T/T_b)^4 > 10^3$ during the undercooling period, one can integrate Eqn. (8), assuming " $T_b \approx 0$ " and $\rho V C_p / 3A\sigma\epsilon_T \approx \text{constant}$, to give:

$$t - t_0 = (\rho V C_p / 3A\sigma\epsilon_T) (T_0^{-3} - T^{-3}), \quad (10)$$

where T_0 is the sample temperature at $t = t_0$. A plot of t vs. T^{-3} is shown in Fig. 13 confirming a linear relationship.

The ESL allows convenient repetition of the superheating-undercooling-recrystallization cycle. This allowed the undercooling temperature for the same 2.3 mm sample of zirconium to be measured for over 100 cycles in about two hours. Fig. 14 shows the normalized cumulative distribution of nucleation events (n_c/N_T) versus the percentage of undercooling.

Summary and Discussion

A high-temperature/high-vacuum electrostatic levitator has been constructed for containerless materials processing. An undercooling experiment with a zirconium sample clearly demonstrates the capability of the system to levitate a dense material stably at high temperature. We have also demonstrated a control of temperature without affecting the position stability, and an open view of the sample for diagnostic measurements. These capabilities will enable a wide range of experiments, which were hitherto impossible, to be conducted on the ground.

So far we have successfully melted and solidified numerous sample materials, including (melting temperatures are shown in parenthesis): In (157 °C), Sn (232 °C), 13i (271.44 °C), Pb (327 °C), In 0.69w% Sb (492.5 °C), Al (670 °C), Ge (938 °C), Cu (1083 °C), Ni (1455 °C), and Zr (1855 °C). In the case of zirconium we have completed more than 400 quantitative undercooling experiments. However, we have not yet demonstrated the capability of processing non-conducting sample materials, an area which we plan to investigate in the near future. We have also limited the processing environment only to high vacuum which has the advantage of ensuring better sample cleanliness. However, for more volatile sample materials a gaseous environment may be more desirable. The heaviest sample that an electrostatic levitator can levitate will be limited by the breakdown voltage of the medium, but this problem will be alleviated in a reduced-g environment where the control voltage can be reduced by several orders of magnitude.

One important practical lesson we have learned is that in order to conduct a successful experiment one must begin with a clean sample (with

reduced volatile contents) and heat it slowly until it reaches thermionic temperatures.

The levitator described in this paper is primarily for Earth-based applications. It can, however, be readily converted for operation in a reduced-g environment. The isotropic force environment of space suggests that an electrode assembly having a tetrahedral symmetry with four spherical electrodes is preferable¹. A lesser control force required in space may allow the possibility of operating in a gaseous environment. The design of a system specifically for space application is currently underway.

Acknowledgements

The authors would like to thank Dr. W. Hofmeister for his guidance in the construction of the silicon pyrometer and Dr. K. Ohsaka for providing us with the alloys used in the present work. This work was carried out at the Jet Propulsion Laboratory, California Institute of Technology, under contract with the National Aeronautics and Space Administration.

References

1. W. K. Rhim, M. Collender, M. '1'. Hyson, W. 'J', Simms, and D. D. Elleman, Rev. Sci. Instrum. **56**, 307 (1985)!
2. C. A. Hahs and R. J. Fox, Proc. 4th Int. Conf. on Exp. Methods for Microgravity Mat. Sci. Research, p23, Ed. R. A. Schiffman (1992).
3. Earnshaw's theorem, see for example S. A. Stratton. Electromagnetic Theory, (McGraw-Hill, New York, p 116, 1941 .)
4. W. K. Rhim, S. K. Chung, E. H. Trinh, and D. D. Elleman, Proc. Mat. Res. Soc. **87**, 329 (1987).
5. W. F. Hofmeister, R. J. Bayuzick, and M. B. Robinson, Rev. Sci. Instrum. **61**, 2220 (1990).
6. J. A. Cadzow and H. R. Martnes, Discrete Time and Computer Control Systems (Prentice Hall, Englewood, NJ) (1970).
7. Achi Brandt, Multi grid Techniques: 1984 Guide, Lecture notes for the Computational Fluid Dynamics Lecture Series, Rhode-Saint-Genese,

Belgium, 26-30 March (1984). W. L. Briggs, A Multigrid Tutorial, Society for Industrial and Applied Mathematics, Philadelphia, PA (1987).

8. E. Ya. Zandberg, and N. I. Ionov, Soviet Phys. Uspekhi, 67,255(1959).

Figure Captions

- Fig. 1. Schematic diagram of an electrostatic levitator in which the sample position is actively controlled only along the vertical direction. It relies on a two-dimensional potential well for centering in the lateral direction.
- Fig. 2. Schematic diagram of the high temperature-high vacuum electrostatic levitator designed for ground-based applications. 1 is the sample, 2 is the electrode assembly, 3 is the focusing lens, 4 is the spherical reflector, 5D and 6D are the position detectors, 5L and 6L are the He-Ne lasers, 7 is the 1 -kW xenon lamp, 8 is the vidco-camera with a telephoto lens, and 9 is the pyrometer.
- Fig. 3. Photograph of the vacuum chamber with a sample being levitated between the electrodes.
- Fig. 4. Schematic diagram of the electrode assembly (side and top views), where 1 is the sample, 2 is the top electrode, 3 is the bottom electrode, 4's are the side electrodes, and 5 is the hole which allows access to the sample storage system.
- Fig. 5. Flowchart of the position control software.
- Fig. 6. User interface display used in the present levitator. The cubical box represents the space between the electrodes in which the sample (the gray dot) moves in search of the set-point (the black dot) by feedback control. The status column displays the sample position, applied high voltages, and the sample temperature. The control parameter column shows the control parameter inputs. The sample position, the control voltage, and the sample temperature are also displayed in the form of oscillograms.
- Fig. 7. (a). Top electrode voltage at the moment of launch versus sample density at three sample diameters. Separation between the top and bottom electrodes is 8 mm.

- (b). Sample charge at the moment of launch versus sample density at three sample diameters.
- Fig. 8. Top electrode voltage needed to levitate the sample midway between the electrodes. The sample charge is assumed to be the same as at launch.
- Fig. 9. (a) Electrode and sample arrangements used in the numerical modeling of the initial 'cold' levitation. (b) The equivalent R-C circuit, which was used to model the dynamic sample charging process under UV irradiation.
- Fig. 10. The steady state sample charge and the required levitation voltage versus α . It was assumed that the sample has a spherical shape and that the steady state charge has been established while it is levitated midway between the electrodes.
- Fig. 11. A photograph of a molten zirconium sample (2.3 mm diameter) being levitated at 2250 K.
- Fig. 12. Temperature versus time as a superheated zirconium drop undergoes radiative cooling.
- Fig. 13. Time versus T^{-3} of the undercooling segment (between 0.3 - 1.6 sec) shown in Fig. 13.
- Fig. 14. Normalized cumulative distribution function versus percentage of undercooling for a 2.3 mm diameter sample of zirconium.

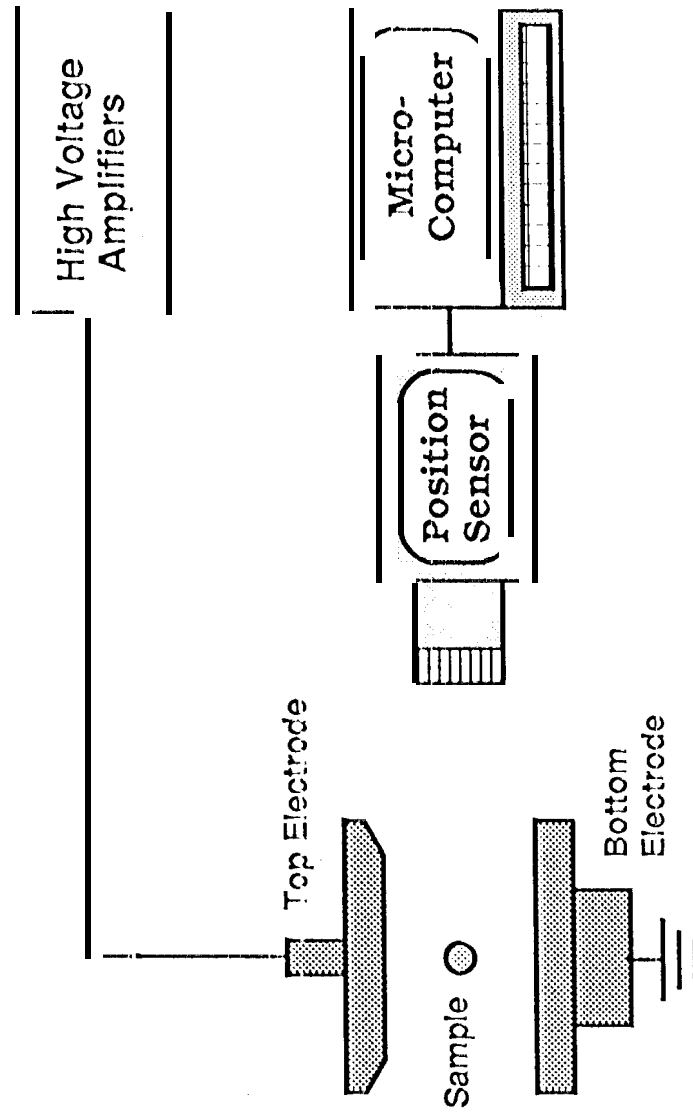


Fig. 1

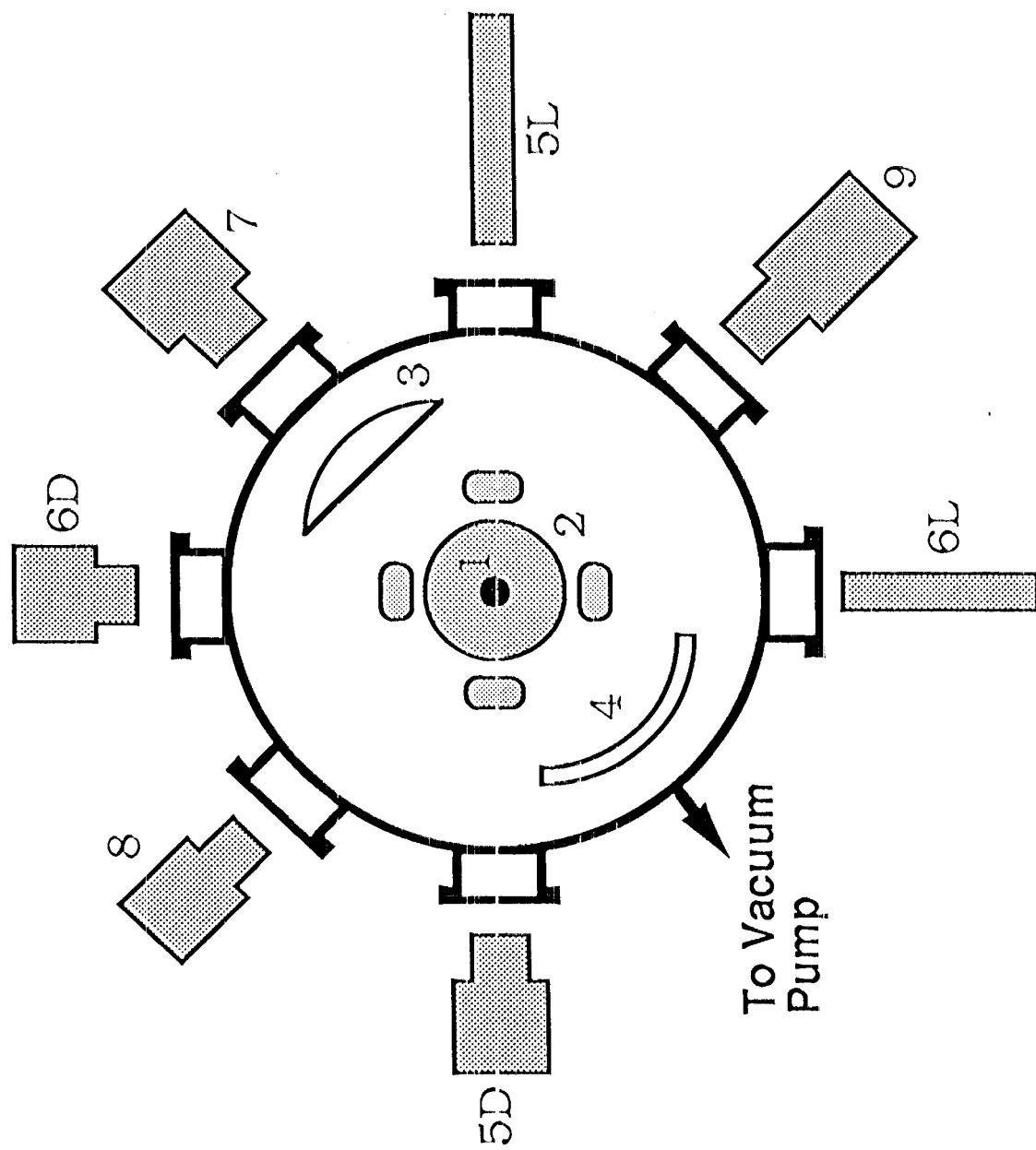
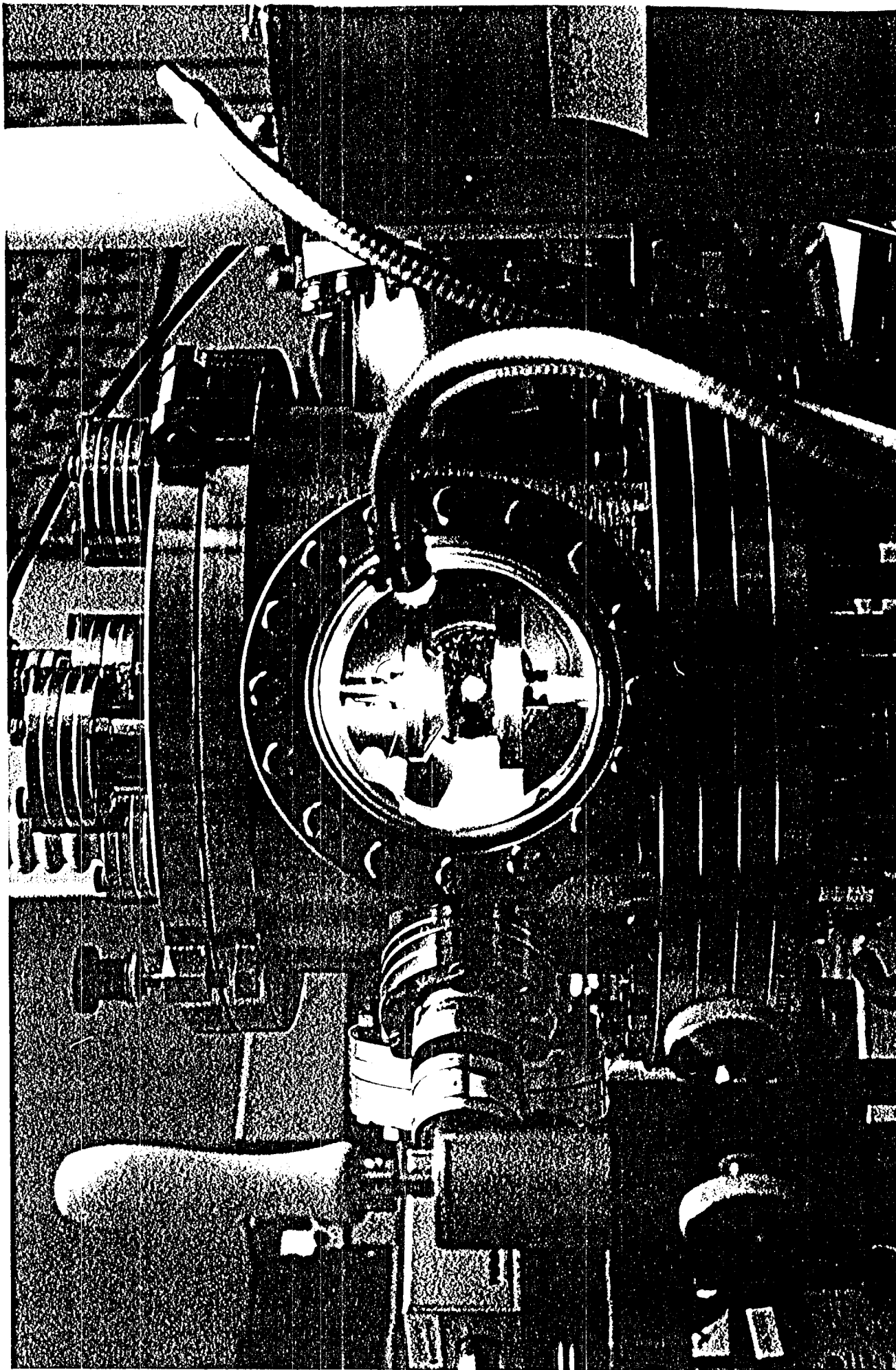


Fig. 2

Fig. 3



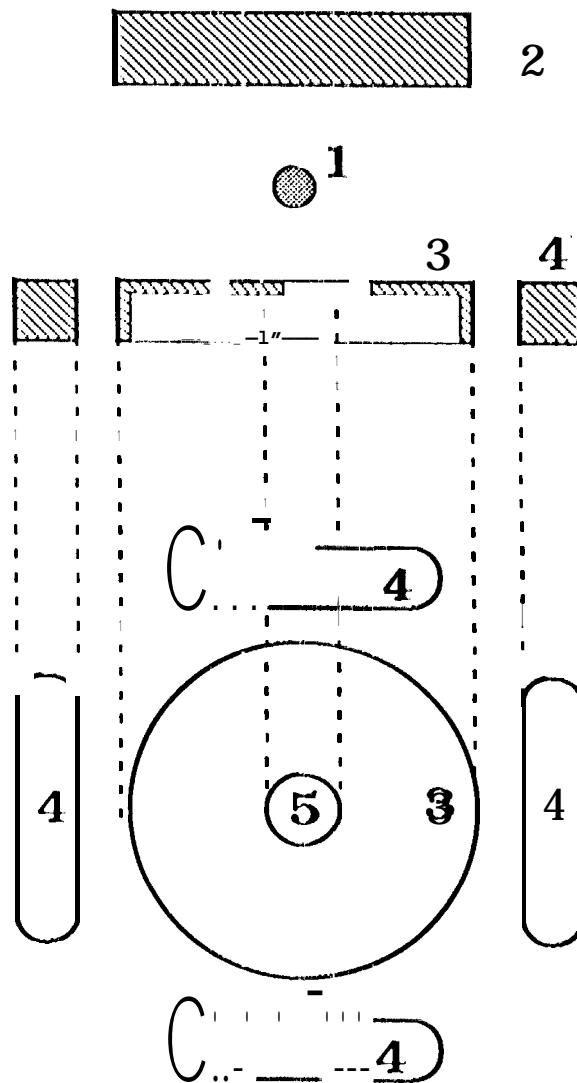
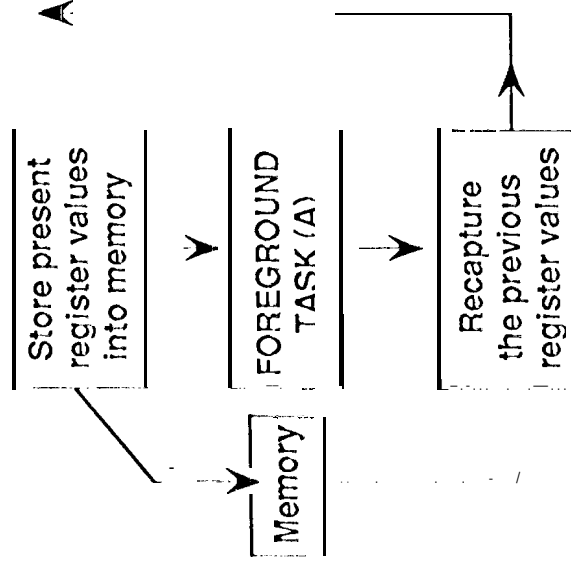
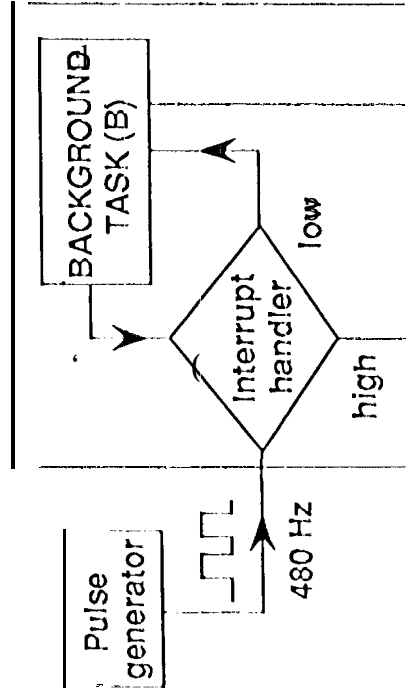
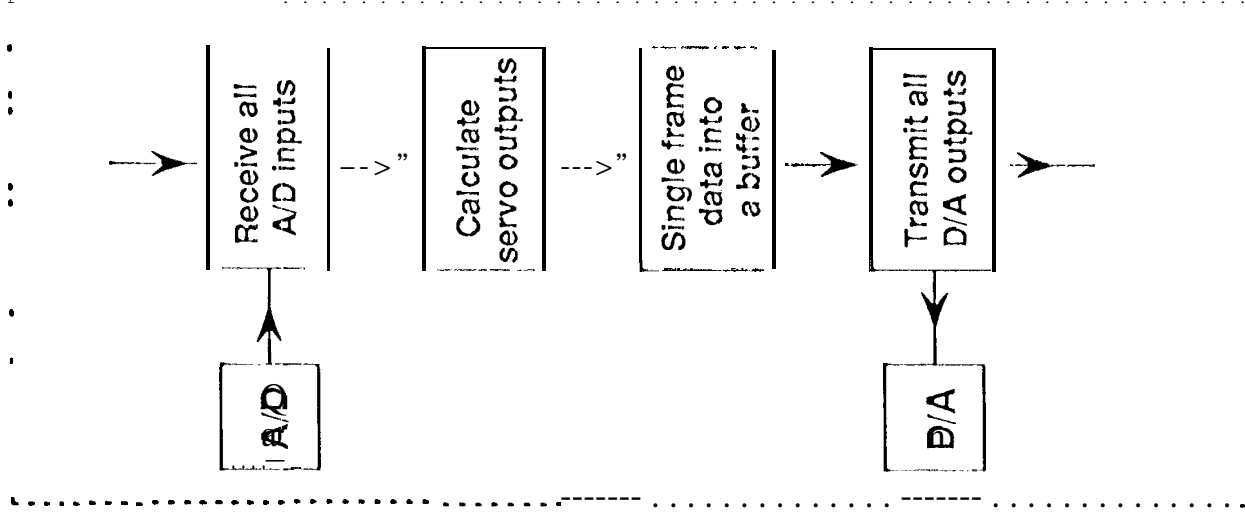


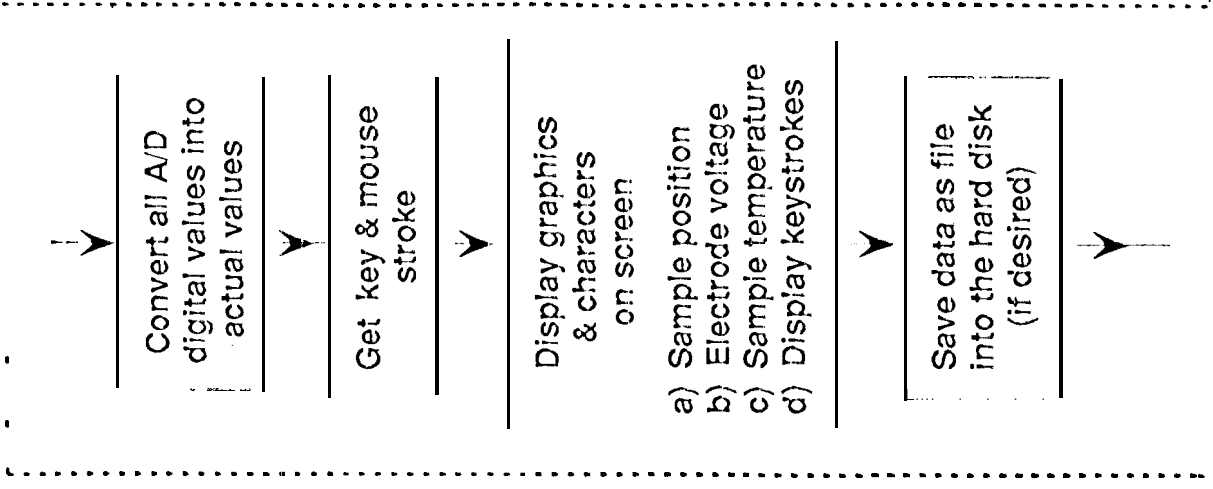
Fig 4



FLOW CHART OF THE SOFTWARE

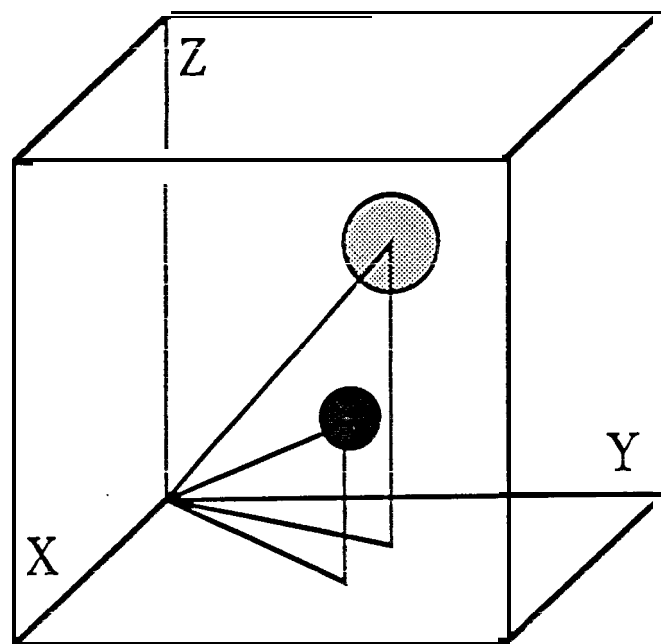


(A) FOREGROUND TASK



(B) BACKGROUND TASK

Fig. 5



Frame Rate 480

Status

X	2040
Y	2052
Z	2021
HV 1	10.2 kV
HV 2	0.2 kV
HV 3	1.2 kV
Temp	1230°

Control Parameters

PG	1200
IG	25
<input checked="" type="radio"/> DG	500
SDG	200
Setp	2021
Frame rate	480

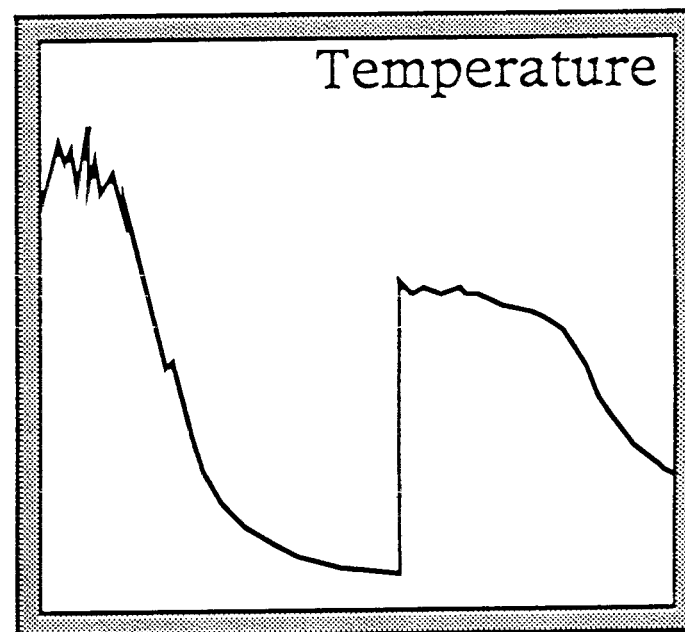
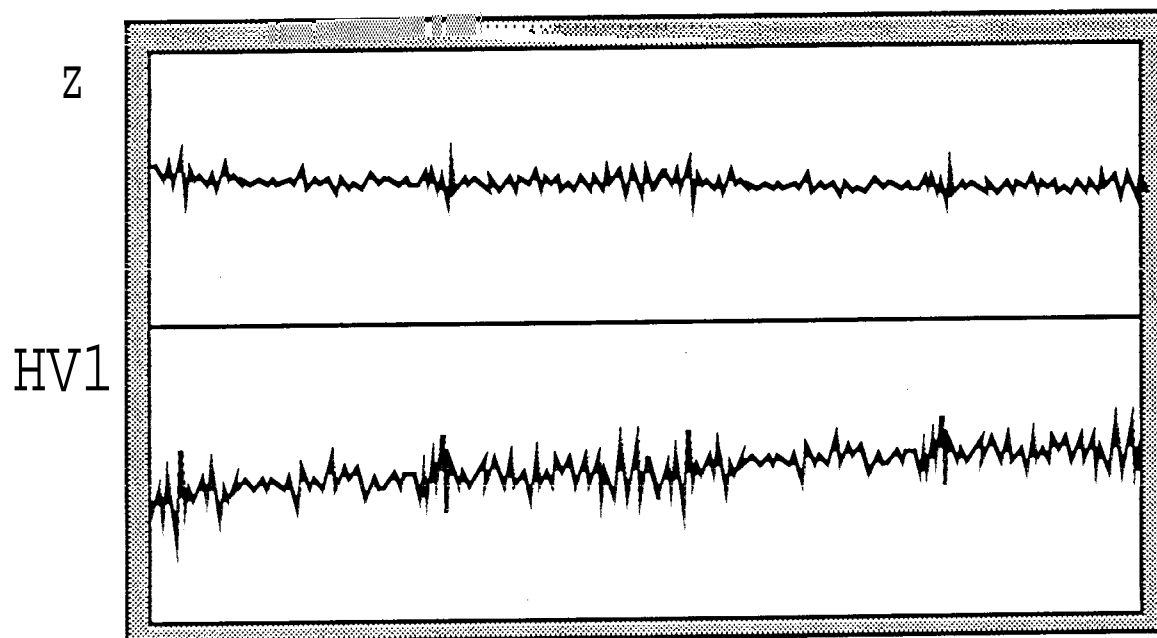


Fig. 6

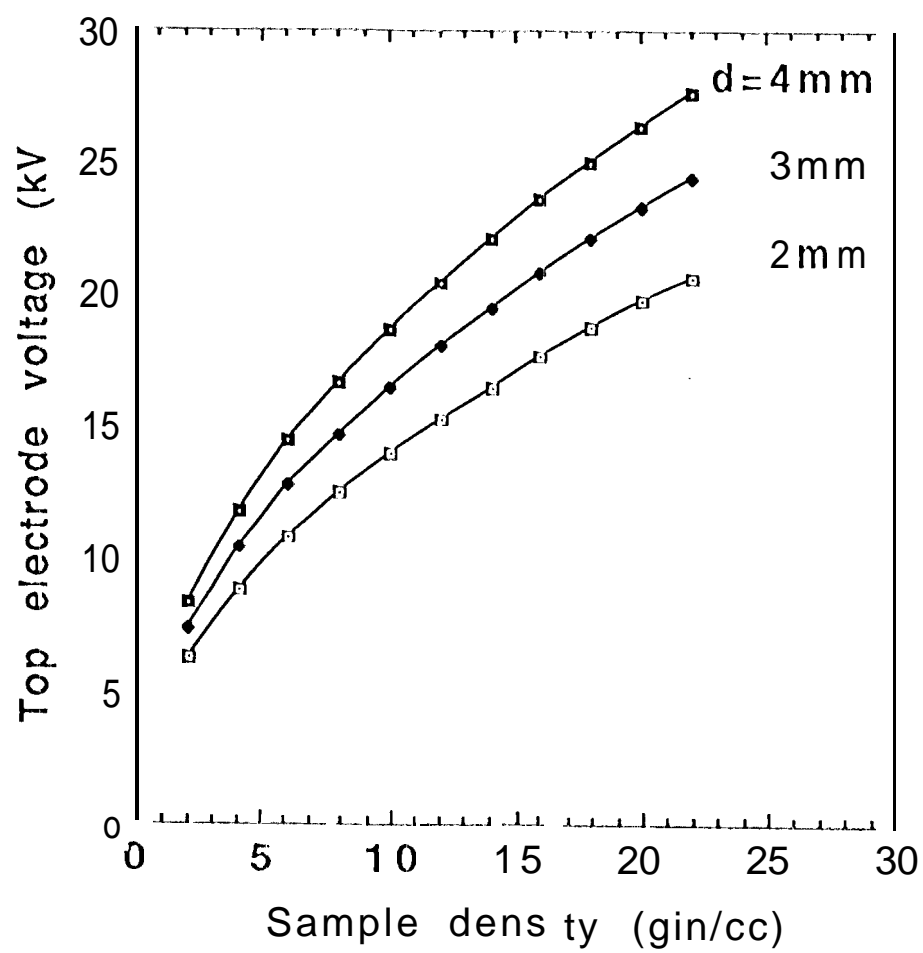


Fig. 7(a)

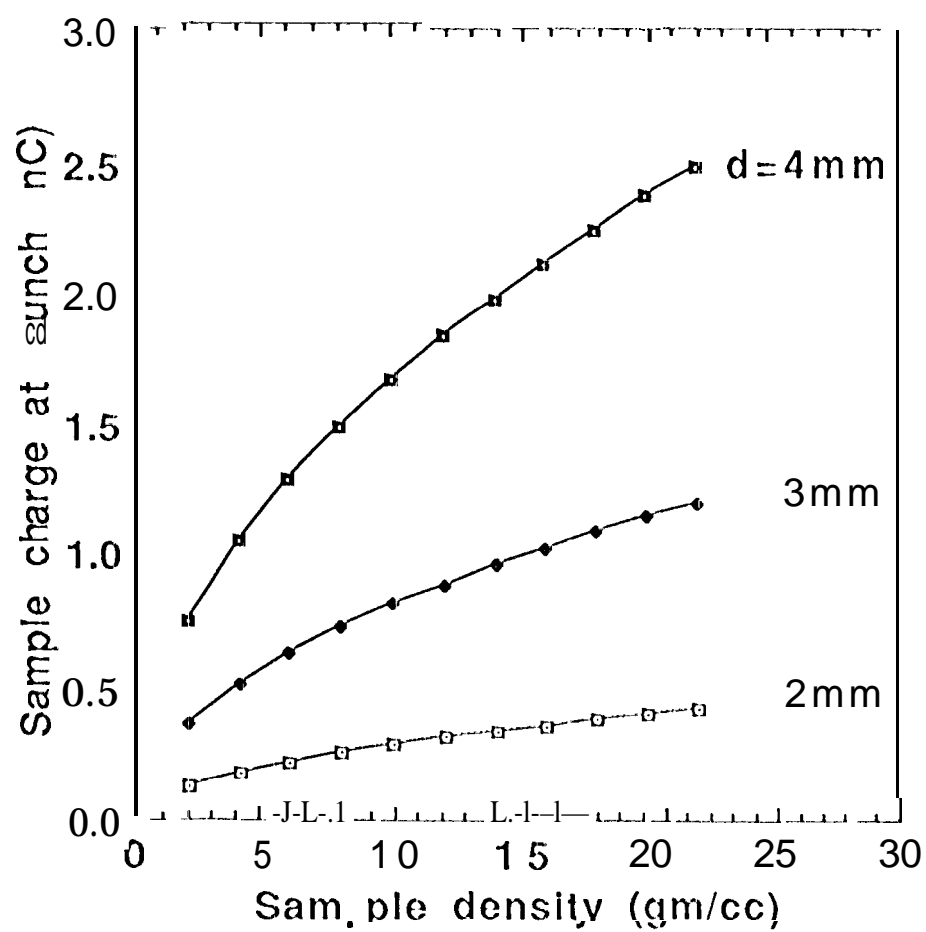


Fig. 7(b)

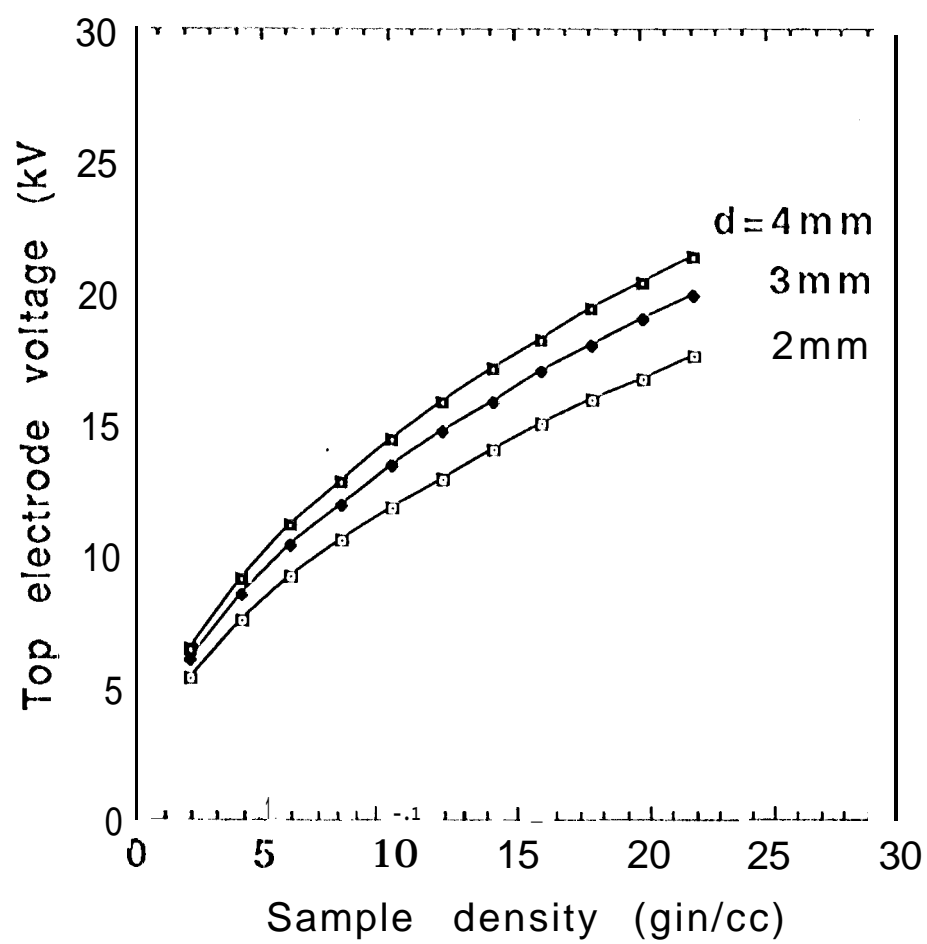


Fig. 8

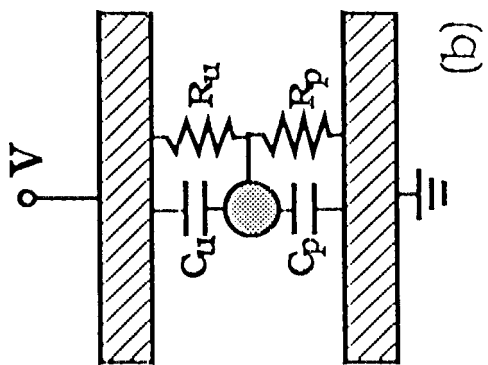
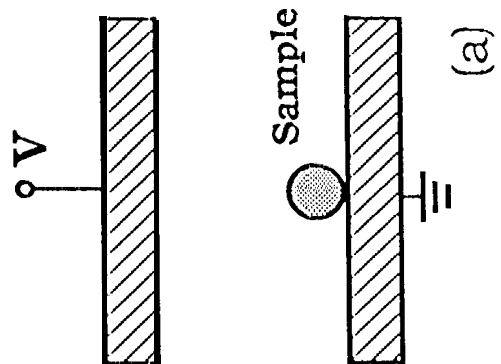


Fig. 9.

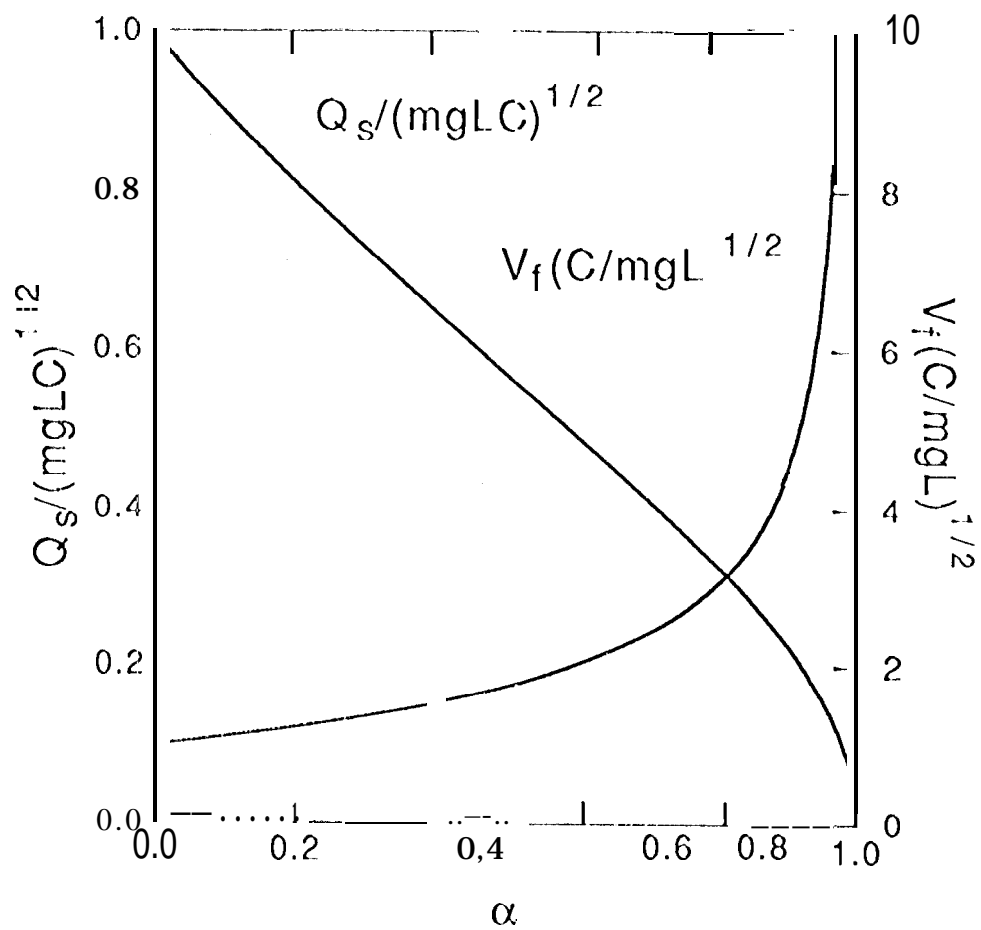


Fig. 11

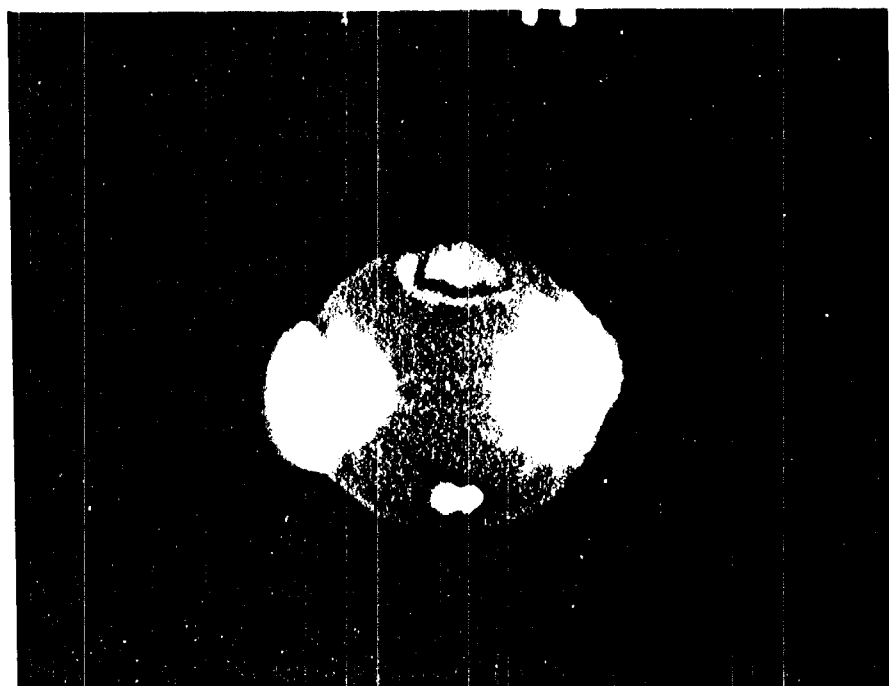


Fig. ¹¹ ~~12~~
Rhim et al

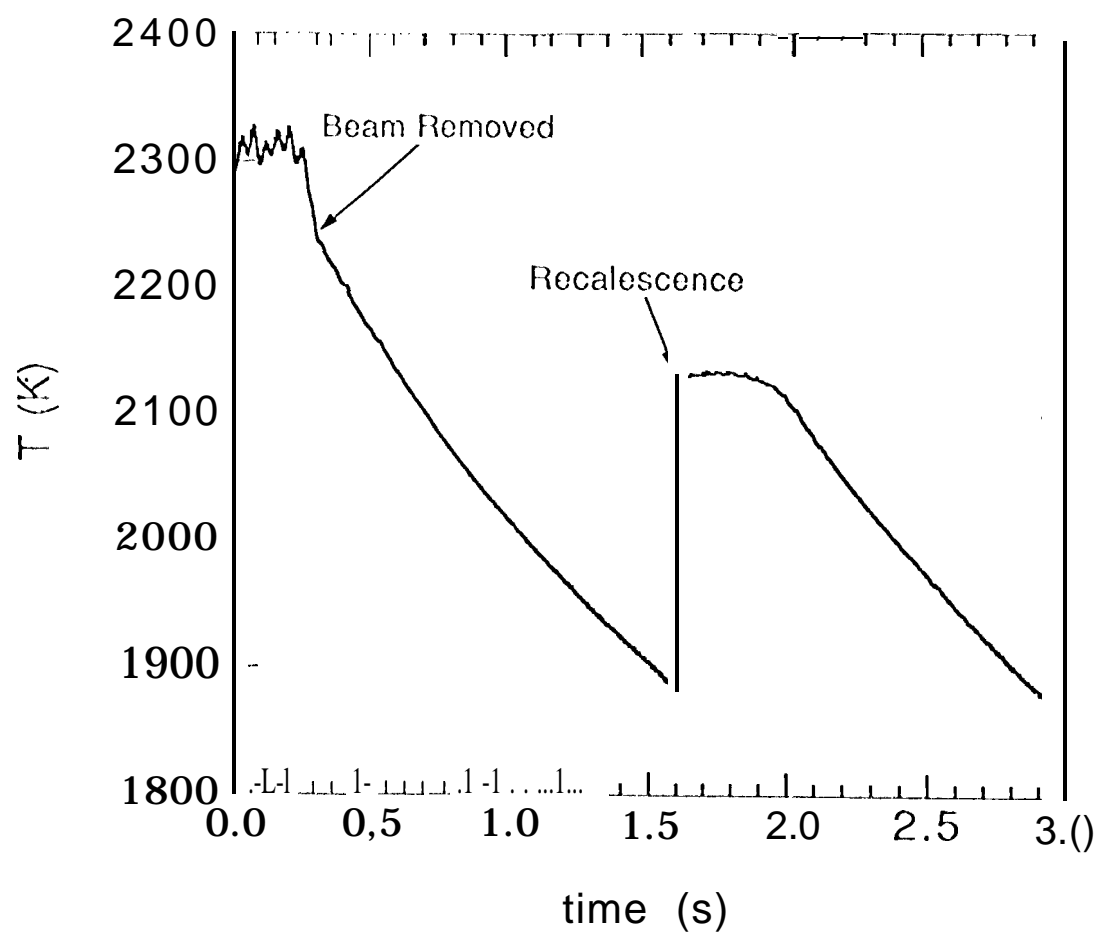


Fig. 12

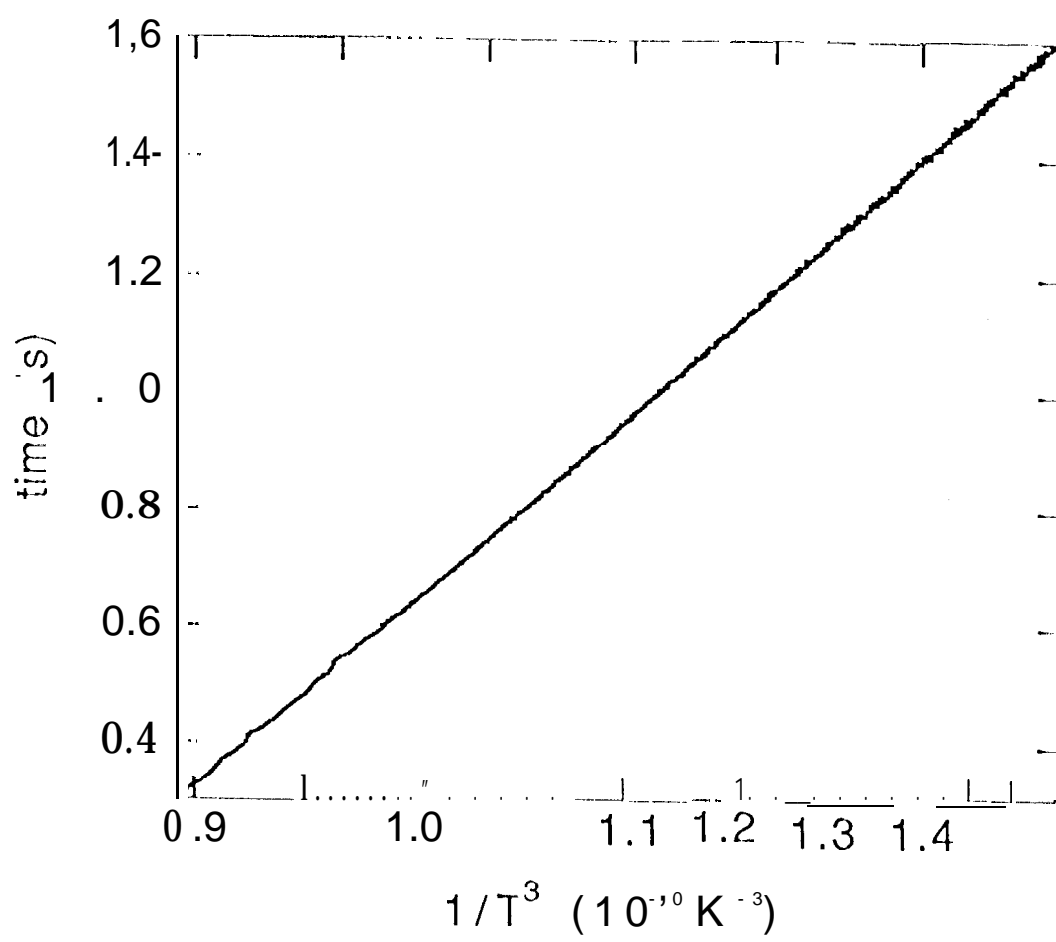


Fig. 13

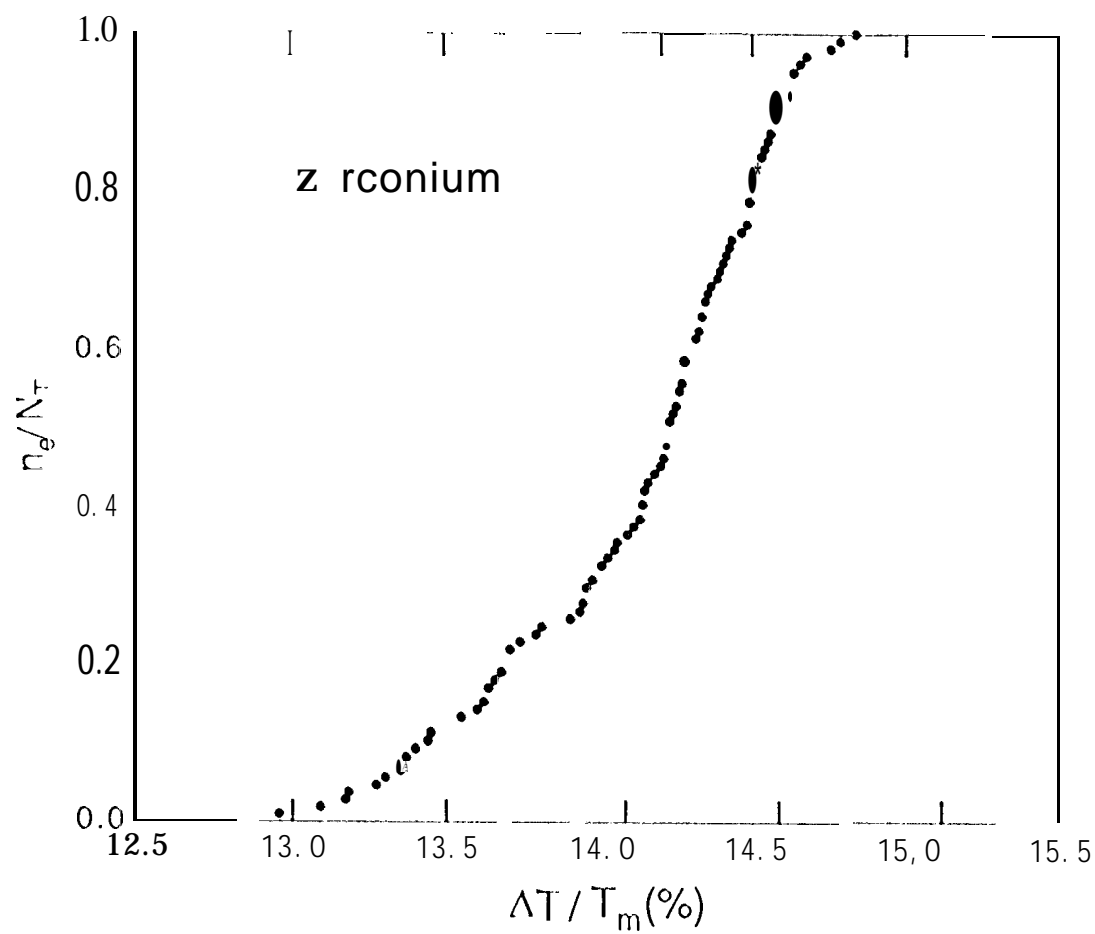


Fig. 14